UNCONVENTIONAL HEXACOPTERS VIA EVOLUTION AND LEARNING: PERFORMANCE GAINS AND NEW INSIGHTS

Jed Muff

Vrije Universiteit Amsterdam
The Netherlands

Keiichi Ito

Vrije Universiteit Amsterdam The Netherlands Elijah H. W. Ang

Technische Universiteit Delft The Netherlands

Karine Miras

Vrije Universiteit Amsterdam The Netherlands A.E. Eiben

Vrije Universiteit Amsterdam The Netherlands

June 12, 2025

ABSTRACT

Evolution and learning have historically been interrelated topics, and their interplay is attracting increased interest lately. The emerging new factor in this trend is morphological evolution, the evolution of physical forms within embodied AI systems such as robots. In this study, we investigate a system of hexacopter-type drones with evolvable morphologies and learnable controllers and make contributions to two fields. For aerial robotics, we demonstrate that the combination of evolution and learning can deliver non-conventional drones that significantly outperform the traditional hexacopter on several tasks that are more complex than previously considered in the literature. For the field of Evolutionary Computing, we introduce novel metrics and perform new analyses into the interaction of morphological evolution and learning, uncovering hitherto unidentified effects. Our analysis tools are domain-agnostic, making a methodological contribution towards building solid foundations for embodied AI systems that integrate evolution and learning.

1 Introduction

Evolutionary computing (EC) is conventionally employed to solve optimization problems, and the research community has developed good tools to analyze the workings of evolutionary algorithms (EA) in this context. This paper considers highly intricate evolutionary systems designed to optimize the *behavior of active*, *embodied agents with autonomy*, rather than merely optimizing a *calculable characteristic of a passive entity*, such as, for example, minimizing tour length for some routing problem. The behavior of an embodied agent is determined by the interactions of its body (morphology), its brain (controller) and its environment. Hence, evolutionary optimization of behavior requires the joint evolution of the agents' bodies and brains, and extending such a system with individual learning has been shown to effectively boost performance [1].

The motivation behind this study lies in the need for high-performing drone designs for various navigation tasks. Our main hypothesis is that evolution can produce non-conventional drone morphologies that outperform the traditional hexacopter design. This will be assessed by considering four different tasks and applying a combination of morphological evolution and reinforcement learning to develop high-performing solutions. Using this approach as a design paradigm is expected to mitigate human biases by decoupling the design process from human intuition, thereby potentially exploring a broader array of possible drone body plans.

The key property of our evolutionary system lies in the distinctive division of adaptation mechanisms between morphology and control: morphologies are evolved, while controllers are not evolved but learned through reinforcement learning. This combination is rare in the evolutionary robotics literature. Most existing systems either evolve both morphology and control or incorporate learning of controllers in addition to evolving them. The latter approach is superior regarding the task performance of the evolved robots, but it can obscure the distinct contributions of each

process. The setup we use here decouples the evolutionary search for body designs from the adaptive shaping of brains, allowing each process to operate in its domain of strength. This setup provides a cleaner separation of timescales and a more interpretable analysis of how morphology facilitates or constrains learning, making our system a valuable contribution to understanding the complementary roles of evolution and learning in embodied intelligence.

2 Related Work

Evolutionary robotics traditionally focused on evolving controllers for fixed robot morphologies [2], yet the concurrent evolution of both morphology and control is becoming increasingly popular. Furthermore, some systems incorporate individual learning that allows new robots to optimize their control systems to effectively improve their inherited morphologies [1, 3, 4].

A generic model behind such systems is the Triangle of Life framework introduced by Eiben et al. [5], which integrates morphological evolution with lifetime learning. In this model, each robot experiences three distinct phases in life: morphogenesis, infancy, and mature life, as illustrated by Figure 1. In this scheme, evolution co-optimizes morphologies and controllers, while learning helps to further optimize the inherited controllers and reach the maximum potential of the given morphologies.

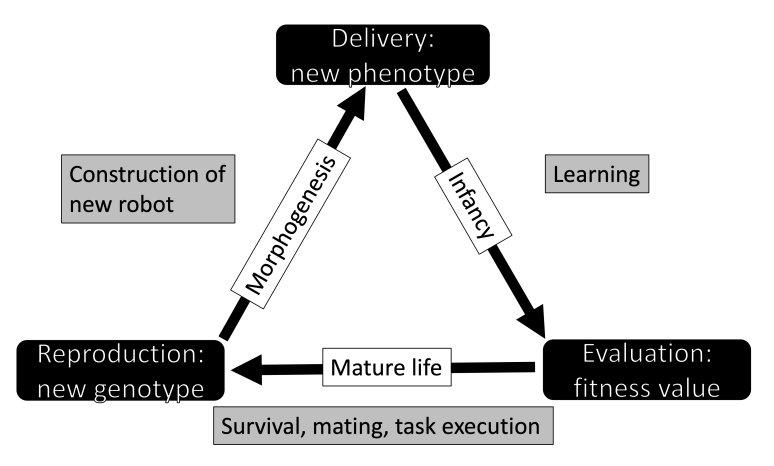


Figure 1: Illustration of the Triangle of Life framework, cf. [5], for evolutionary robotics underpinning the setup used in this paper.

Cheney et al. [6] investigated the co-evolution of morphology and control of soft robots, enhanced by a technique called Morphological Innovation Protection that temporarily reduces selection pressure on recently produced individuals. Although the authors did not explicitly distinguish the evolution of the body and the learning of the brain, their system can be considered as an instantiation of the Triangle of Life model with a specific approach to the infancy phase. The main result of the paper is the demonstration that the Morphological Innovation Protection mechanism delays premature convergence and stagnation, resulting in substantially higher fitness values.

Miras et al. [3] compare two approaches to creating good controllers for evolving modular robots, that is, "evolution only", in which controllers are inherited together with morphology, and "evolution plus learning", in which a robot's controller is inherited, but additionally, it is enhanced by a learning method. Their experiments showed that not only the second approach generated a higher fitness but also that the morphologies were different compared to evolution-only results. This result is remarkable, considering that the two setups only differ in the manner they treat controllers; yet, the difference between the outcomes is clearly observable in the evolved morphologies. However, the most interesting contribution of this study is the introduction and the analysis of the learning delta: the performance gain obtained by learning in the infancy phase. This measure captures the learning ability of a given robot body that can be interpreted as its morphological intelligence. The experiments showed that the learning delta is growing over consecutive generations.

Jelisavcic et al. [4] and Luo et al. [7] investigated a particularly tight integration of evolution and learning by means of Lamarckian evolution. Both papers highlighted the benefit of Lamarckian inheritance (genetic transmission of traits acquired through learning) and Luo et al. also showed a greater increase in learning delta compared to Darwinian evolution.

Paper	Morphology Evolution	Controller Evolution	Controller Learning
Jelisavcic et al. (2017)	√	√	√
Cheney et al. (2018)	\checkmark	\checkmark	\checkmark
Miras et al. (2020)	\checkmark	\checkmark	\checkmark
Gupta eta al. (2021)	\checkmark	×	\checkmark

Le Goff et al. (2023) Luo et al. (2023)

Table 1: Quick overview of papers on evolution and learning in Evolutionary Robotics

A special combination of evolution and learning can be obtained by deactivating the evolution of controllers in the Triangle of Life. In the resulting system, the evolutionary process is restricted to morphologies, with controllers being optimized exclusively through learning.

One such system was investigated by Gupta et al. [8] who introduced a computational framework called deep evolutionary reinforcement learning (DERL) and demonstrated the link between environment complexity and morphological intelligence that facilitates learning and the morphological Baldwin effect. Tasks that were time-consuming to learn in the early generation were achieved in a shorter time in later generations. Let us note that they defined morphological intelligence by the ability to learn new tasks, while learning delta in Miras et al., related it to the given task for which robots are being evolved.

Another example can be found in the study of Le Goff et al. [9] who investigated the evolution and learning of robots with particular attention to the acceleration of learning. They did not evolve controllers but learned a new controller for each newly generated morphology. To accelerate learning, they used a controller archive that stored successful controllers associated with specific robot types (defined by their morphological features). If the type for a 'newborn' morphology exists in the archive, then the stored controller associated with this type is used to initialize the learning process. In essence, this enables a 'warm start' of learning relying on an archive, instead of using the inherited controller for this purpose.

Morphology Controller Automatic Asymmetrical Paper Optimization Optimization Navigation Designs Behjat et al. (2020) Limited × Sufiyan et al. (2021) Limited \times Zeng et al. (2022) Limited \times Bergonti et al. (2024) X X Ang et al. (2025) X

Table 2: Quick overview of papers on drone optimization

All the above work illustrates the benefit of learning in the infancy stage for morphologically evolving robots. Within the specific field of co-optimization of morphology and control of a drone with learning, one paper was found, Behjat et al. [10] proposed a novel metric, Talent, to estimate the learning capacity of a given morphological design using principles from control theory - without requiring the actual learning process. They also introduced "capacity variables", which are surrogate design variables to reduce the number of variables and make them all continuous in optimization. Their experiments focused on a basic task: achieving stable take-off and hover, rather than addressing more complex behaviors like navigation.

The co-design of drone morphology and its swarm behavior was investigated by Zeng et al. [11]. They developed on the concept of the talent metrics of Behjat and proposed a framework that concurrently searches for the robot morphology and the hyper-parameters (i.e., talent metrics) of their behavior model that jointly optimize the collective (team) performance of autonomous search of signal source.

Bergonti et al. [12] proposed a co-design of winged-drone morphology (wing roots are actuated and can morph in-flight) and control, whose design parameters include topology, actuation, morphing strategy, and controller parameters. They compute optimal trajectories for each of their morphologies. However, these are not automatic navigation policies, but are control inputs that are optimized to perform a prescribed scenario that includes obstacle avoidance.

Sufiyan et al. [13] investigate a unique drone configurations: "lift is achieved by spinning its entire body with attached airfoils around a central axis and positional control is attained through regulation of 2 sets of independent aerodynamic

surfaces and thrusters." They investigate the co-evolution of two species, one is the mechanical design variables and the other is Proportional-Integral-Derivative (PID) controller and Central Pattern Generator (CPG) variables.

For the evolution of drones, we see that there is a gap in research of co-optimization of morphology and controllers, particularly ones involving learning of navigation. Table 2 summarizes the points of interest of the relevant literature in drone co-optimization.

3 Problem description: drones and tasks

The problem we consider is the design of hexacopter drones that can perform various navigation tasks.

3.1 Design space: hexacopcter drones

The complete design problem can be naturally decomposed by distinguishing two major components of a drone.

- The physical body (morphology) of the drone. This consists of a central unit and the arms. The central unit contains the battery, the power distribution board, the flight controller, and some sensors such as the Intertial Measurement Unit (IMU) or cameras. The six arms are attached to the central unit, each holding a electronic speed controller, motor and propeller.
- The brain (controller) of the drone. This is the software running on the flight controller to drive the drone. The specific function of the brain is to generate control commands to each of the motors.

Crucially, the behavior of a drone is determined by it's body and brain together. This implies that optimizing a drone's task performance requires the joint optimization of both it's body and brain.

As mentioned before, we choose to employ different mechanisms to optimize the bodies and the brains. Bodies will be optimized by evolution. From this perspective, a drone morphology is a phenotype and specifying an evolutionary algorithm requires defining appropriate genotypes (representation of the phenotypes), reproduction operators to produce new genotypes from existing ones, and selection operators to regulate mating and survival. These elements and the overall fitness function will be described in Section 4.

To optimize brains, we will use reinforcement learning to produce a policy for controlling the motors. How a policy is represented and how it is optimized will be described in Section 5.

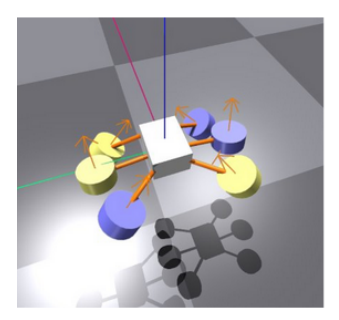


Figure 2: Hexacopter type drone to illustrate the design space of morphologies.

3.2 Tasks

We consider four tasks shown in figure 3: a circular track where the goal is to travel in a circle, a slalom track where the goal is to weave in and out along a line like a snake, a shuttlerun task where the drone has to fly back and forth between two gates, and an infinity track or Figure 8 track.

These tasks will be interfaced with the optimizers via a fitness function for evolution and a reward function for reinforcement learning.

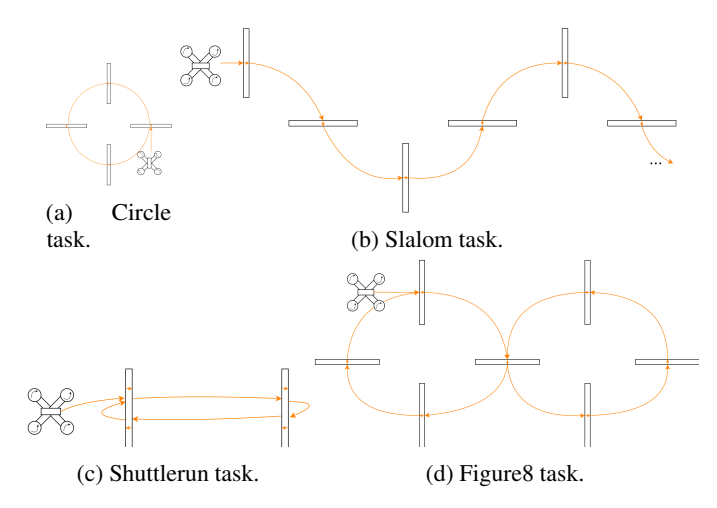


Figure 3: Diagrammatic representation of the tasks (using a quadrocopter for illustration).

4 Evolution

We use an evolutionary algorithm following the $(\mu + \lambda)$ scheme known in evolution strategies [14]. In this scheme, μ is the population size, λ is the offspring size and the + means that after reproduction the best μ individuals to form the next generation are selected from the union of all parents and offspring.

4.1 Initial Population

The initial population of drones is created randomly. However, this cannot be done naively as it also leads to a number of drones that cannot fly due to not enough thrust in a single direction to compensate gravity. To prevent wasting time on 'non viable' drones, we use a mathematical static hovering test as described in [15] to filter them out in order to initially only generate drones that can fly.

The static hovering problem is defined as a minimization problem as follows,

$$\begin{aligned} & \min & \hat{\mathbf{u}}^T \hat{\mathbf{u}} \\ & \text{s.t.} & ||\mathbf{B}_{\mathbf{F}} \hat{\mathbf{u}}||_2 = g \\ & \mathbf{B}_{\mathbf{M}} \hat{\mathbf{u}} = \mathbf{0} \\ & \mathbf{u} < \hat{\mathbf{u}} < \overline{\mathbf{u}}. \end{aligned} \tag{1}$$

where $\hat{\mathbf{u}} \in \mathbb{R}^n$ is the optimal control input vector from the control input space $\mathbf{u} \in \mathbb{R}^n$ which minimizes the hovering cost. For drones, the control input \mathbf{u} is equal to the square of the propeller rotational speed, ω^2 . $\mathbf{B_F} \in \mathbb{R}^{3 \times n}$ and $\mathbf{B_M} \in \mathbb{R}^{3 \times n}$ are the specific force and moment effectiveness matrices, respectively. The first equality constraint ensures that the optimal control input $\hat{\mathbf{u}}$ produces a specific force sufficient to overcome gravity, while the second equality constraint ensures that this control input produces zero moments. The inequality constraint ensures that $\hat{\mathbf{u}}$ remains within the lower (\mathbf{u}) and upper $(\overline{\mathbf{u}})$ control limits.

4.2 Representation

We represent the morphology of a drone as a two-dimensional list, each subarray representing an arm-motor combination with 6 parameters given in table 3.

All together, a hexacopter is represented by 36 parameters. Figure 4 shows the effect of these parameters on the drones' morphologies.

4.3 Mutation Operator

Our evolutionary process is based solely on mutation, as preliminary experiments revealed that the crossover operators implemented tended to hinder optimization. The reason for this diminished performance is due to the low locality, in which small genotypic changes result in large phenotypic changes. It is well established that evolutionary algorithms benefit from encodings with high locality [16, 17, 18]. Our mutation strategy respects this principle by limiting drastic

Parameter	Range	Description
l	[0.09, 0.4] m	Arm length; motors are always placed at the end of the arm, facing upward along the z-axis.
ψ_a	$[0,2\pi]$ rad	Arm polar rotation angle (anticlockwise).
θ_a	$[-\pi,\pi]$ rad	Arm azimuth rotation angle. Positive z-axis is upward.
ψ_m	$[0,2\pi]$ rad	Motor polar rotation angle (anticlockwise).
$ heta_m \ dir$	$[-\pi,\pi]$ rad $\{0,1\}$	Motor azimuth rotation angle. Binary value indicating direction of motor spin.

Table 3: Parameter definitions, ranges, and descriptions used in the mutation operator.

Table 4: Mutation parameters used in the evolutionary algorithm. $(\mu + \lambda)$ evolutionary strategy was used with $\mu = 12$ and $\lambda = 12$ and 40 generations. Note the probability values represent a distribution which combine to 1.

Parameter	Probability to Mutate	Scale of Mutation
l	0.19	0.1
ψ_a	0.19	0.2
$egin{array}{c} \psi_a \ heta_a \ \psi_m \end{array}$	0.19	0.2
ψ_m	0.19	0.2
θ_m	0.19	0.2
dir	0.05	-

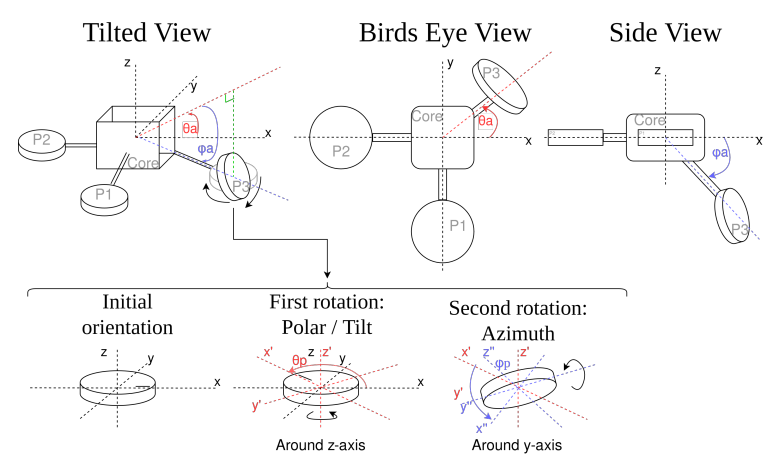


Figure 4: Schematic image of a drone with three arms and propellers to illustrate the effect of the parameters that represent the body layout.

changes through probabilistic control. Mutation occurs on an individual **A** which is represented as a matrix of n arms, each with m parameters. First, an arm is selected by uniform selection $i \sim \mathcal{U}(\{1,\ldots,n\})$ and then mutating one of its parameters $j \sim \mathbf{x}$, chosen according to a fixed probability distribution \mathbf{x} shown in table 4). The lower probability assigned to the direction parameter dir reflects its disproportionate impact on the phenotype.

For nondirectional parameters, sampled Gaussian noise $\mathcal{N}(0,\sigma)$ is added, followed by clipping or wrapping to maintain valid bounds (arm lengths are clipped to their limits and angles are wrapped to $[0,2\pi]$). The value of σ for each parameter is shown in table 4. For the direction parameter, mutation simply flips its binary value. Finally, a repair operator \mathcal{R} is applied to ensure that the mutated structure remains valid and collision-free; this repair operator is explained in Section 4.4.

This mutation operator is mathematically expressed in equations 2.

$$i \sim \mathcal{U}(\{1, \dots, n\}) \quad j \sim \mathbf{x}$$

$$\mathcal{M}(\mathbf{A})_{i,j} = \begin{cases} \operatorname{clip}(a_{i,j} + \epsilon), & \text{if } j \neq m \\ 1 - a_{i,j}, & \text{if } j = m \end{cases} \quad \text{where } \epsilon \sim \mathcal{N}(0, \sigma)$$

$$\mathbf{A}' = \mathcal{R}(\mathcal{M}(\mathbf{A}))$$
(2)

Here, $a_{i,j=m}$ denotes the motor spinning direction dir.

4.4 Repair Operator: Ensuring Rotor Separation

To ensure that evolved drone configurations are physically viable and would remain operational in real-world conditions, we introduce a geometric repair operator that enforces minimum spatial separation between rotors. Specifically, we prevent rotor overlap by modeling each motor as occupying a three-dimensional bounding box centered on its position. The dimensions of each bounding box are defined by the rotor geometry: the width and depth correspond to the diameter of the propeller D, and the height is set to 2H, where H is the height of the propeller. The increased vertical space accounts for aerodynamic downwash and minimizes rotor interference.

Let $\mathbf{m}_i \in \mathbb{R}^3$ denote the 3D position of motor i, and let $\mathsf{bbox}_i \in \mathbb{R}^3$ represent its bounding box. The goal of the repair operator is to iteratively resolve any collisions between pairs of bounding boxes (bbox_i , bbox_j) by applying repulsive displacement vectors to the motor positions. For any overlapping pair (i,j), the motors are displaced along the vector connecting their centers:

$$\mathbf{m}_{i}' \leftarrow \mathbf{m}_{i} - \alpha \cdot \hat{\mathbf{d}}_{ij}, \quad \mathbf{m}_{j}' \leftarrow \mathbf{m}_{j} + \alpha \cdot \hat{\mathbf{d}}_{ij}$$
 (3)

Here α is a small step size, and the process is repeated iteratively until all the bounding boxes do not overlap. This ensures that all drones respect real-world spacing constraints between rotors, thereby improving the realism of the designs.

4.5 Fitness function

Following the Triangle of Life model, the fitness of a drone is evaluated after the learning period, using the inherited body and the learned brain. The fitness is defined as the number of waypoints the drone passes during the evaluation period, which is set at 12 seconds throughout this paper. Note that this definition is independent of the specific task; as long as the task is formulated by means of waypoints, this definition is simply applicable.

5 Reinforcement Learning

Reinforcement Learning (RL) is a paradigm in which an agent learns to make decisions by interacting with an environment in order to maximize cumulative rewards. At each timestep t, the agent observes a state, selects an action, receives a reward r_t , and transitions to a new state. The agent's goal is to learn a policy that maximizes the expected return, defined as the sum of future rewards:

$$G_t = \sum_{k=0}^{\infty} \gamma^k r_{t+k},\tag{4}$$

where $\gamma \in [0, 1]$ is a discount factor that prioritizes immediate rewards over distant ones.

We employ Proximal Policy Optimization (PPO) [19], a widely used policy gradient method that directly adjusts the policy parameters to maximize the expected return. PPO follows an actor-critic framework: a policy network (actor) proposes actions based on the current state, while a value network (critic) estimates the expected return from that state.

Training proceeds by collecting *rollouts*, sequences of states, actions, and rewards gathered by running the current policy in the environment. Instead of updating after each individual interaction, PPO accumulates a batch of rollout data and optimizes the policy over several epochs using *mini-batches* — randomly sampled subsets of the collected data. This improves sample efficiency and stabilizes learning.

PPO maximizes a clipped surrogate objective that limits the size of policy updates, ensuring more stable and conservative improvements. Its combination of simplicity, robustness, and efficiency makes it particularly suitable for continuous control tasks in robotics.

For all tasks used in this study, a single simple reward function is used as shown in Equation 5. It can be intuitively understood as the velocity the drone travels towards the next gate plus some penalty for rotating too much. This penalty is needed to guide the learning process to begin with, so that the drone can learn to hover. The specific formula is given by the following equation

$$r_t = (s_{t-1} - s_t) - 0.001 \cdot \|\mathbf{\Omega}_t\| \tag{5}$$

where

- r_t is the reward at timestep t.
- s_t is the distance to the next gate at timestep t.
- Ω_t is the rotational velocity at timestep t.

The observation the drone receives contains 16 variables: 3 for position of the drone relative to the next gate, 3 for velocity of the drone relative to the next gate, 3 for the Euler angle of the drone, 3 for the angular velocity of the drone, and finally a further 4 for the relative position and yaw of the next gate with respect to the current target gate.

The computational budget for learning a policy is 2.5×10^8 time steps. This value was chosen because it was the minimum number of training steps needed for the conventional hexacopter design to learn the tasks.

Note that the reward function used for learning and the fitness function to drive evolution are different. This was chosen because fitness is meant to reflect the overall task performance (which is captured well by the number of waypoints), whereas RL needs a reward function that provides frequent and informative feedback to guide learning over short timescales.

Table 5: PPO Hyperparameters used for training. Parameters not listed here are kept at their Stable-Baselines3 [20] defaults.

Parameter	Value
Policy Architecture	3-layer MLP, (64, 64, 64) units
Activation Function	ReLU
Log Std Init (for policy)	0
$n_{ m steps}$	1000
Batch Size	5000
$n_{ m epochs}$	2.5×10^{8}
Discount Factor (γ)	0.999
Learning Rate	0.0003 (default)
GAE Lambda (λ)	0.95 (default)
Clip Range	0.2 (default)
Entropy Coefficient	0.0 (default)
Value Function Coefficient	0.5 (default)
Max Gradient Norm	0.5 (default)
Use SDE (State-Dependent	
Exploration)	False (default)
Number of Environments	
Simulated at once	100

6 Experiment setup

The principal algorithm for developing high-performance drones blends evolution and learning, organized hierarchically as per the Triangle of Life model outlined in Section 2.

In the evolutionary process, drone morphologies undergo reproduction and selection, without directly considering the controllers. That is to say, controllers are not represented by the genotypes; hence, they are not inheritable, and thus they are not evolvable.

Controllers for newly produced drones are provided by RL in the Infancy stage, the second side of the triangle. Crucially, the fitness of a drone morphology is determined after this learning stage, and it is this fitness value that drives the morphology evolution process. Thus, even though drone controllers are not directly evolvable, evolution does take notion of them.

A multirotor drone simulator is implemented in Python3 and is used to train the reinforcement learning policy and evaluate the fitness values. We used a similar simulator as in the work of Ferede et al. [21]. The dynamics of the drone is given as,

$$\dot{\mathbf{p}} = \mathbf{v}$$

$$\dot{\mathbf{v}} = g\mathbf{e}_3 + \mathbf{R}(\mathbf{\Theta})\mathbf{F}$$

$$\dot{\mathbf{\Theta}} = \mathbf{Q}(\mathbf{\Theta})\mathbf{\Omega}$$

$$\dot{\mathbf{\Omega}} = \mathbf{M}$$

$$\dot{\boldsymbol{\omega}} = \tau^{-1}(\boldsymbol{\omega}_c - \boldsymbol{\omega})$$
(6)

where $\mathbf{p} \in \mathbb{R}^3$ is the position vector in inertial reference frame, $\mathbf{v} \in \mathbb{R}^3$ is the velocity vector in inertial reference frame, $\mathbf{\Theta} \in \mathbb{R}^3$ are the Euler angles representing the drone's orientation and $\mathbf{\Omega} \in \mathbb{R}^3$ is the angular velocities. $\boldsymbol{\omega} \in [0,1]^n$ and $\boldsymbol{\omega_c} \in [0,1]^n$ are the normalized actual and commanded propeller speeds for the n propellers, respectively. $\mathbf{R}(\mathbf{\Theta})$ represents the rotation matrix that projects vectors from body reference frame to inertial reference frame. g is the gravitational acceleration, 9.81 m/s², and τ is the propeller time constant, set as 0.01 s.

The specific forces and moments, F and M, are given in body reference frame, given as,

$$\mathbf{F} = \mathbf{B}_{\mathbf{F}} \boldsymbol{\omega}^2$$

$$\mathbf{M} = \mathbf{B}_{\mathbf{M}} \boldsymbol{\omega}^2$$
(7)

The equations of motion are numerically integrated using the Forward-Euler method with a timestep size of $\Delta t = 0.01$ s.

7 Human versus evolved designs

Here we present and discuss the outcomes of the experiments from the perspective of the first research question: how are the evolved drones compared to the usual design? We break this down into two related sub-questions: how do they perform and how do they look.

7.1 Task performance of evolved designs

The first issue we investigate is how the task performance of evolved drones compares to the usual drone design. Table 6 presents a summary of the findings. The most important results (shown in light grey cells) indicate that the evolved drone designs greatly outperform the traditional hexapod on all tasks. The degree of enhancement varies by task, with improvements ranging from 29% on the Circle task (increasing from 34 to 44) to 170% on the Shuttle run task (rising from 10 to 27).

Task	Metric	Traditional	Evolved
		drone	drone
Circle	Task performance	34	44
	Max. reward achieved	72.0	69.1
	Average lap time	0.83	0.70
Slalom	Task performance	29	41
	Max. reward achieved	65.0	72.5
	Average lap time	1.02	0.87
Shuttle	Task performance	10	27
run	Max. reward achieved	30.2	89.8
	Average lap time	3.04	1.38
Figure8	Task performance	14	34
	Max. reward achieved	22.3	65.0
	Average lap time	1.87	0.88

Table 6: Comparison between the traditional hexacopter and the best evolved hexacopters. Task performance is measured by the number of waypoints the drone passes during the evaluation period.

Figure 5 provides a detailed picture, showing how fitness changes over the course of the evolutionary process. Although applying evolutionary algorithms for drone design is a new application area, the evolutionary dynamics are as usual.

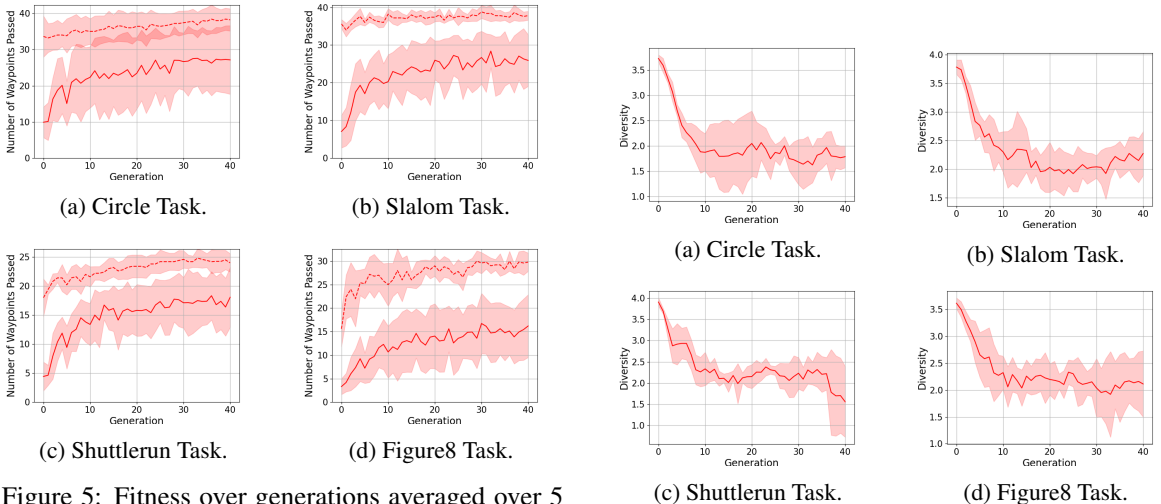


Figure 5: Fitness over generations averaged over 5 runs. Solid lines: average fitness, dotted lines: maximum fitness.

Figure 6: Diversity over generations averaged over 5 runs.

Looking at the performance improvement in the different benchmark tasks we can observe the following. The circle and slalom tasks exhibited only marginal gains throughout the evolutionary process. On the other hand, the shuttle run and figure8 tasks demonstrated more substantial enhancements in fitness values. For the circle task, progress appeared slow, but the fitness did not stagnate, indicating a continuous, albeit gradual, exploration of the design space. Throughout the four tasks, the algorithm maintains its capacity to identify improved solutions over time.

By means of an extra sanity check, we also inspect how population diversity changes over the course of evolution. Figure 6 displays the related plots. For these plots we define population diversity by the level of novelty of the individuals in it, and the notion of novelty is defined by the genotypic distance between two individuals.

To quantify the difference between two individuals, we define an *edit distance* based on the spatial configuration of their arms. Each individual is represented as a two-dimensional array of parameters, where the first dimension indexes the arms and the second dimension contains their associated features. Let $\mathbf{A} = \{\mathbf{a}_1, \dots, \mathbf{a}_n\}$ and $\mathbf{E} = \{\mathbf{e}_1, \dots, \mathbf{e}_n\}$ be two such individuals, each with n arms and m-dimensional parameter vectors $\mathbf{a}_i, \mathbf{e}_i \in [0, 1]^m$.

The edit distance $D(\mathbf{A}, \mathbf{E})$ is computed as follows:

- 1. Normalize all arm parameters to lie within [0, 1].
- 2. Compute the pairwise cost matrix $C \in \mathbb{R}^{n \times n}$ where each entry is the Euclidean distance between one arm \mathbf{a}_i from \mathbf{A} and another arm \mathbf{b}_j from \mathbf{B} :

$$C_{ij} = \|\mathbf{a}_i - \mathbf{e}_j\|_2 \tag{8}$$

3. Solve the assignment problem to find a bijection $\pi: \{1, \dots, n\} \to \{1, \dots, n\}$ that minimizes total cost:

$$D(\mathbf{A}, \mathbf{E}) = \sum_{i=1}^{n} \|\mathbf{a}_i - \mathbf{e}_{\pi(i)}\|_2$$
(9)

This is solved efficiently using the Hungarian algorithm [22].

Novelty for an individual $\bf A$ is calculated as the normalized average edit distance to all other individuals ${\bf E}^{(1)},\ldots,{\bf E}^{(\mu)}$ in the population:

$$N(\mathbf{F}) = \frac{1}{\mu} \sum_{i=1}^{\mu} \frac{D(\mathbf{A}, \mathbf{E}^{(j)})}{D_{\text{max}}}$$
(10)

where D_{max} is the maximum pairwise edit distance observed in the current population, used for normalization.

Diversity of a population is defined as the average novelty of all individuals in that population:

$$Div = \frac{1}{\mu} \sum_{i=1}^{\mu} N(\mathbf{A}^{(i)})$$
 (11)

All evaluated tasks showed relatively rapid decline in population diversity as seen Figure 6. This trend underscores possible dependence of the initial population in navigating the search space.

Given the relatively high-dimensional design space and the significant computational resources required for each evaluation, the total number of evaluations were limited. Despite these limitations, our findings demonstrate that the proposed algorithm can indeed discover designs that outperform the conventional design. We do not assert the optimality of our method. However, this work provides a foundation, showcasing the potential of evolutionary algorithms to generate superior designs, and indicating a need for future research focused on enhancing exploration strategies and mitigating the impact of initial population bias in such complex design problems.

7.2 Morphology of evolved designs

Figure 7 presents drones with top performance for each task. These were selected through a lexicographic ordering based on the achieved fitness and novelty. That is, selection was done in two steps for each task independently. Firstly, the set of top-performing drones was identified. (The exact performance figures are given in Table 6.) Secondly, these drones were ranked by their novelty, defined as the total edit distance from all other individuals (see above). Figure 7 illustrates the highest-ranking drones, which simultaneously optimize for task performance and novelty.

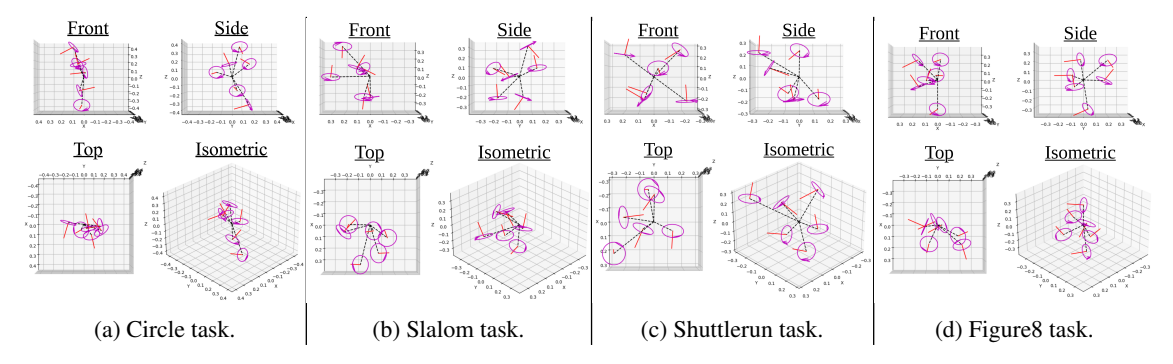


Figure 7: The best evolved drone for each task maximizing task performance and novelty at the same time.

The most apparent property of the drones displayed in Figure 7 is their irregularity. In other words, they all have a nonconventional morphology. Their layout is not symmetrical, and even closer inspection cannot reveal an intuitive logic behind their shapes. To look into this aspect closer, we consider the symmetry of the drones' morphologies. We define two measures to quantify body symmetry as follows: central point symmetry and bilateral yz-plane symmetry. In both cases we define the set of 3D points as $P = \{\mathbf{p}_1, \mathbf{p}_2, \dots, \mathbf{p}_n\} \subset \mathbb{R}^3$ representing an individuals geometric configuration. Central point symmetry is evaluated by comparing the vectors made by the arms to their reflections through the origin. For each point $\mathbf{p}_i \in P$, the *central reflection through the origin* is defined as: $\mathbf{p}_i' = -\mathbf{p}_i$

Then, for each \mathbf{p}'_i , compute the Euclidean distance to its closest neighbor in P: $d_i = \min_{\mathbf{q} \in P} \|\mathbf{p}'_i - \mathbf{q}\|$. Then the **central symmetry score** is the mean of these minimum distances:

$$CeS(P) = \frac{1}{n} \sum_{i=1}^{n} d_i = \frac{1}{n} \sum_{i=1}^{n} \min_{\mathbf{q} \in P} \| -\mathbf{p}_i - \mathbf{q} \|$$
 (12)

The bilateral symmetry is similar; however, the points are reflected across the yz-plane. The yz plane was chosen because the positive y direction signifies the forward direction for each task. To reflect each point \mathbf{p}_i across the yz-plane, you simply $\mathbf{p}'_i = (-x_i, y_i, z_i)$.

The bilateral symmetry score is defined as the average minimum distance from each reflected point to the closest point in the original set:

$$BiS_{yz}(P) = \frac{1}{n} \sum_{i=1}^{n} \min_{\mathbf{q} \in P} \|\mathbf{p}_{i}' - \mathbf{q}\|$$
(13)

Both metrics equal 0 if and only if every point in P is perfectly reflected across the origin or yz plane, respectively. Larger values indicate an increasing deviation from this ideal.

Figure 8 shows the development of symmetry over generations of the slalom task, as an example. Remarkably, the CeS values are increasing, indicating an evolutionary disadvantage of central symmetry. This does not hold for BiS values; bilateral symmetry is more of less constant. This may suggest some kind of invariance that we are currently not aware of. Although the issue of body symmetry is beyond the scope of this paper, these results are interesting to present for future investigations.

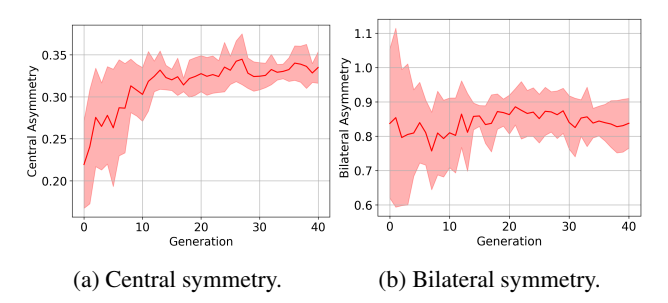


Figure 8: The evolution of body symmetry for the slalom task. Higher values indicate less symmetrical bodies.

8 The interplay of evolution and learning

To appreciate the results comparing human and evolved designs, recall that the task performance of a drone (the number of waypoints it passes during the evaluation period) is determined after training a control policy by RL using the same computational budget for all morphologies and all tasks. This means that our approach tacitly converts the question

"How good is this morphology?"

into another question

"How good can this morphology be made by learning a controller for it?"

In the following, we take a deep dive into this issue.

8.1 Metrics for Analyzing Learning Dynamics

To characterize the learning process, we define a series of quantitative metrics based on the episodic reward signal. These metrics are computed based on a smoothed version of episodic rewards, denoted \tilde{r}_t , obtained using a median sliding window aggregation over a fixed-size window of 1000 episodes.

The key idea behind these metrics is to define two important moments during the learning process and divide the full learning period into three stages accordingly, the early stage, the mid stage and the late stage. Figure 9 illustrates the main concepts visually.

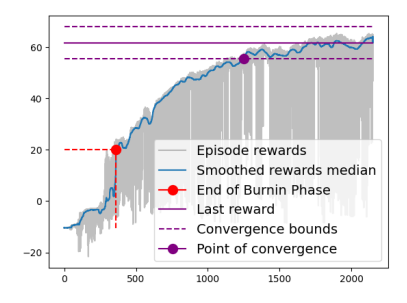


Figure 9: Example of how a learning curve looks and what the learning descriptors represent.

The first stage that we call the burn-in phase is the period of quick wins where the rewards are growing rapidly. Technically speaking, the **Point of Burn-in** (t_b) is defined as the timestep at which the maximum positive change in the

smoothed reward curve occurs:

$$t_b = \operatorname*{arg\,max}_t \Delta \tilde{r}_t,\tag{14}$$

where $\Delta \tilde{r}_t = \tilde{r}_{t+1} - \tilde{r}_t$ denotes the first difference of the smoothed reward series.

Recall that the reward function used in this paper reflects the velocity the drone travels towards the next gate. Thus, intuitively, the burn-in phase is the period of learning to fly, that is, acquiring the basic skill to perform the task at hand.

The second important moment is the **Point of Convergence** (t_c) , defined as the earliest timestep after which the smoothed rewards remain within a fixed relative tolerance $(\pm 10\%)$ of the final reward \tilde{r}_T . Formally, this is not the end of learning, but improvements after this point are relatively small. One could say that after this point, drones are only fine-tuning their behavior.

Next we define a metric to reflect the progress made over the time interval between the point of burn-in and the point of convergence. The **Learning Speed** (s) is quantified as the maximum reward achieved during the mid stage of the learning period divided by the duration of that period:

$$s = \frac{\tilde{r}_{\text{max}}}{t_c - t_b},\tag{15}$$

Note that learning speed is a relative metric because the maximum reward is pertained to the length of a time interval. Therefore, it reflects the efficiency of learning. An absolute measure to evaluate learning efficacy is the **Maximum Reward Achieved** (\tilde{r}_{max}), defined as the maximum smoothed episodic reward achieved during training:

$$\tilde{r}_{\max} = \max_{t} \tilde{r}_{t}. \tag{16}$$

The last metric we introduce is not related to efficiency, nor to efficacy. Instead, it indicates how stable the learning process is. We capture this feature by defining **Learning Volatility** $(\sigma_{\Delta \tilde{r}})$ as the mean absolute difference between consecutive smoothed episodic rewards:

$$\sigma_{\Delta \tilde{r}} = \frac{1}{T - 1} \sum_{t=0}^{T - 2} |\tilde{r}_{t+1} - \tilde{r}_t|. \tag{17}$$

In the following, we investigate the interplay of evolution and learning by considering the development of these metrics over consecutive generations.

8.2 Analysis of Learning Dynamics

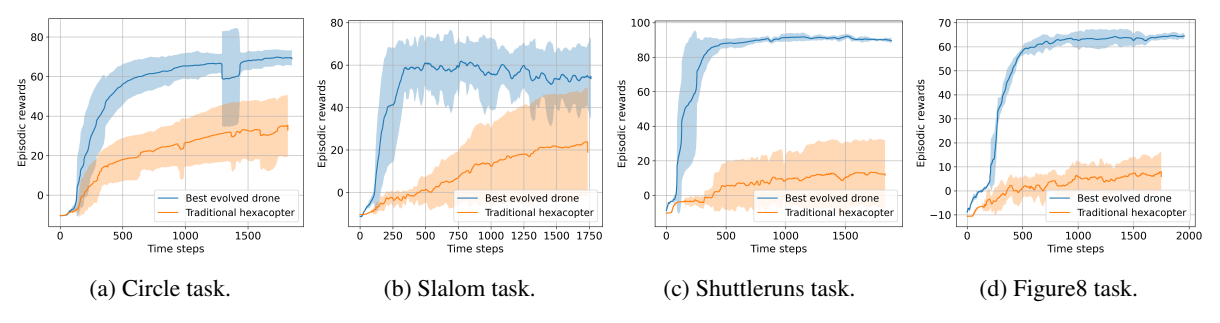


Figure 10: The episodic reward plot over simulation timesteps for the conventional hexacopter design and the best designs shown in figure 7, averaged and smoothed over 10 runs.

The data presented in the previous section demonstrated the superiority of the task-performing behavior of the evolved drones compared to the traditional hexacopter. In this section, we look at their learning behavior. To this end, we compare the learning dynamics of the traditional hexacopter and the best evolved drone per task.

Figure 10 highlights the substantial performance gains of the evolved drone morphologies compared to the conventional hexacopter. Notably, the learning curves exhibit a sharper trajectory, characterized by a rapid and efficient burn-in phase followed by stable convergence. Figures 11, 12, 13, and 14 further illustrate the progression of learning throughout the evolutionary process. The consistently low standard deviation across runs indicates a clear and repeatable trend: evolved individuals are becoming increasingly proficient learners. Specifically, learning occurs more rapidly (Figure

12), and higher maximum rewards are achieved (Figure 11). However, this improvement comes with a trade-off. On the one hand, learning is becoming less stable with increasing levels of volatility, suggesting that small policy changes have a growing impact on performance. On the other hand, the duration of the burn-in phase is decreasing, indicating that the selected morphologies are those capable of acquiring fundamental flight behaviors more quickly.

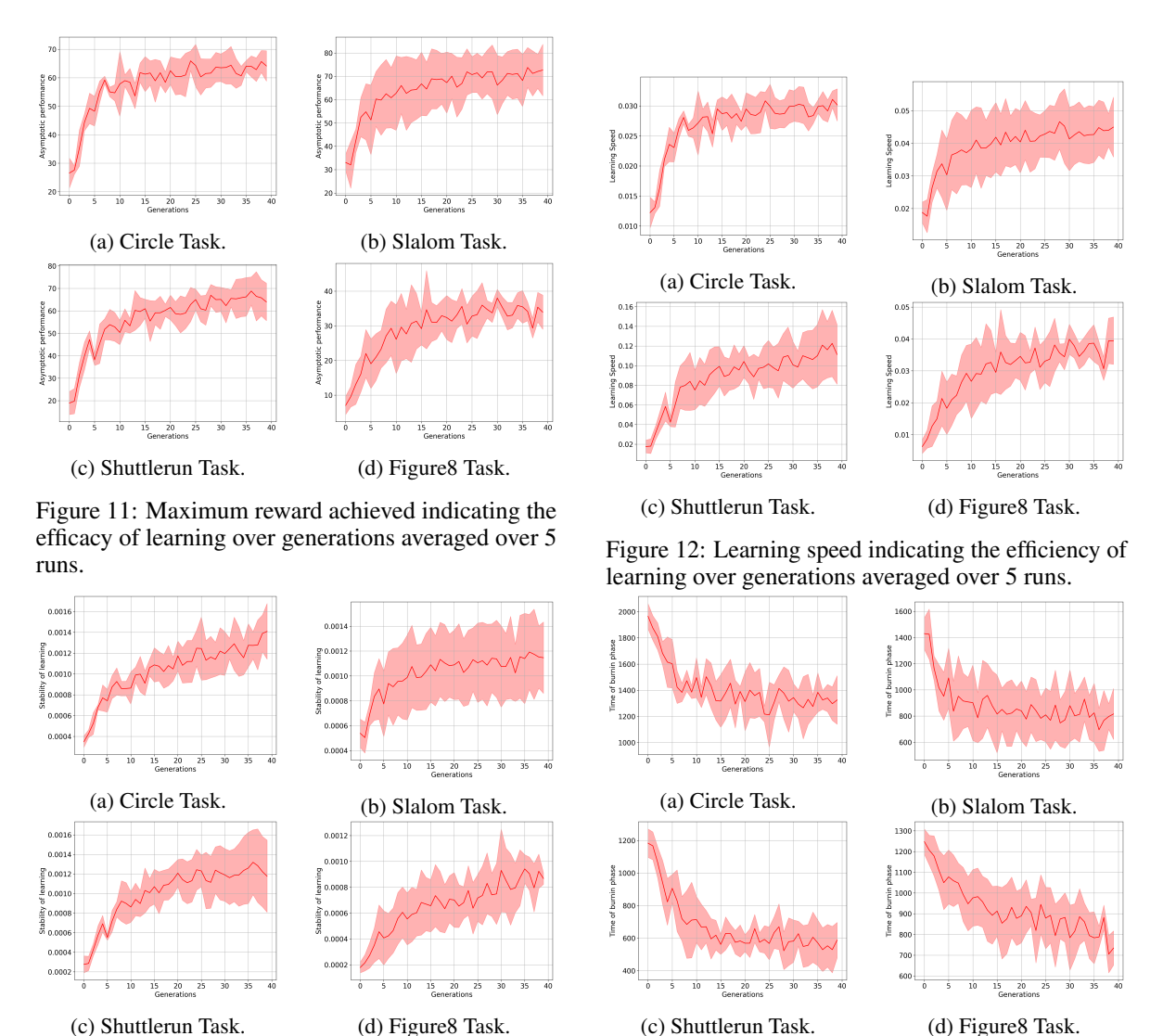


Figure 13: Volatility of learning over generations averaged over 5 runs.

Figure 14: Point of burn-in over generations averaged over 5 runs.

Taken together, these findings suggest that the evolved designs demonstrate improved morphological intelligence, enabling them to learn effective controllers with reduced effort. This is fully in line with the literature as established in Miras et al [3] where the phenomenon of increasing learning deltas was shown first. However, it is worth noting the great differences in system setup. In [3] learning had a 'warm start' since it started from the inherited controller, and the reward function used in the learning algorithm was identical to the fitness function used by evolution. The method in this paper uses a 'cold start' since controllers are not inheritable (nor do we have an archive as in [9]), and the reward function used by the learning method is different from the fitness function. The latter feature is not a matter of user preference; it is a consequence of using reinforcement learning. Reinforcement learning inherently uses fine-grained rewards per time step, whereas the optimization methods employed as learners for evolvable morphologies use a coarse-grained evaluation calculating the quality of robot behavior just once, after the complete evaluation period is finished [23]. Last but not least, the robots (hexacopters), the tasks (Section 3.2) and the environment (air), investigated here are completely different from the modular robots evolved for crawling locomotion on the ground used in the other related papers.

Given these differences, the emergence of the same pattern –namely, that evolution tends to produce morphologies which support more efficient learning– across such divergent systems is striking. It suggests that the observed synergy between morphological evolution and lifetime learning is not merely a byproduct of specific algorithmic or environmental choices. Rather, it points to a deeper underlying phenomenon: a universal principle whereby evolution discovers structural priors that facilitate learning during an individual's lifetime. This convergence across systems with different embodiments, learning paradigms, and reward structures indicates that we are tapping into a fundamental aspect of embodied intelligence, capturing something intrinsic about the co-adaptation of body and brain.

9 Concluding Remarks

This paper introduced a novel framework for co-optimizing the morphology and control of drones through the combined use of evolutionary algorithms and reinforcement learning. Our primary contribution is the demonstration that evolved, non-conventional drone morphologies –when paired with task-specific learned controllers– can significantly outperform the standard hexacopter design across a range of navigation tasks. These findings provide evidence that decoupling the optimization of body and brain, and tailoring the learning process to each evolved morphology, can unlock high-performance solutions beyond the reach of human design intuition.

A second, equally important contribution lies in the introduction of a general-purpose methodological toolbox to analyze the interaction between evolution and learning. The metrics developed to characterize learning dynamics (burn-in time, learning speed, volatility, and maximum reward) enable a principled, quantitative analysis of how morphology affects learnability. This toolbox is domain-agnostic and can support investigations in a wide range of embodied AI systems that combine evolution with learning.

Beyond these technical contributions, our findings raise interesting theoretical questions. For instance, the observation that evolved drones tend to exhibit lower symmetry despite improved performance challenges conventional assumptions about the role of symmetry in design. Additionally, the apparent selection for morphologies that are 'easier to learn' suggests an emergent form of morphological bias induced by the learning process. This phenomenon warrants deeper exploration.

Future work will investigate the impact of explicit symmetry constraints, the dynamics of morphological canalization, and the potential of Lamarckian learning schemes. Moreover, applying this framework to real-world hardware will help validate the transferability of evolved morphologies.

10 Acknowledgments

The research reported in this paper was supported by the European Commission Horizon project SPEAR, EU grant number 101119774, https://www.spear-robotics.com/.

References

- [1] J. Luo, A. Stuurman, J. Tomczak, J. Ellers, and A.E. Eiben. The effects of learning in morphologically evolving robot systems. *Frontiers in Robotics and AI*, 8, 2022.
- [2] Shanker G. Radhakrishna Prabhu, Richard C. Seals, Peter J. Kyberd, and Jodie C. Wetherall. A survey on evolutionary-aided design in robotics. *Robotica*, page 1–18, 2018.
- [3] Karine Miras, Matteo De Carlo, Sayfeddine Akhatou, and A. E. Eiben. Evolving-controllers versus learning-controllers for morphologically evolvable robots. In Pedro A. Castillo, Juan Luis Jiménez Laredo, and Francisco Fernández de Vega, editors, *Applications of Evolutionary Computation 23rd European Conference, EvoApplications 2020, Held as Part of EvoStar 2020, Seville, Spain, April 15-17, 2020, Proceedings*, volume 12104 of *Lecture Notes in Computer Science*, pages 86–99. Springer International Publishing, 2020.
- [4] Milan Jelisavcic, Rafael Kiesel, Kyrre Glette, Evert Haasdijk, and A. E. Eiben. Analysis of Lamarckian evolution in morphologically evolving robots. In Carole Knibbe, Guillaume Beslon, David P. Parsons, Dusan Misevic, Jonathan Rouzaud-Cornabas, Nicolas Bredèche, Salima Hassas, Olivier Simonin, and Hédi Soula, editors, *Proceedings of the Fourteenth European Conference Artificial Life, ECAL 2017, Lyon, France, September 4-8, 2017*, pages 214–221. MIT Press, 2017.
- [5] A.E. Eiben, N. Bredeche, M. Hoogendoorn, J. Stradner, J. Timmis, A.M. Tyrrell, and A. Winfield. The triangle of life: Evolving robots in real-time and real-space. In Lio P., Miglino O, Nicosia G, Nolfi S, and Pavone M., editors, *Proc. 12th European Conference on the Synthesis and Simulation of Living Systems*, pages 1056–1063. MIT Press, 2013. triangle-2013.

- [6] Nick Cheney, Josh Bongard, Vytas SunSpiral, and Hod Lipson. Scalable co-optimization of morphology and control in embodied machines. *Journal of The Royal Society Interface*, 15(143):20170937, 2018.
- [7] Jie Luo, Karine Miras, Jakub Tomczak, and Agoston E. Eiben. Enhancing robot evolution through Lamarckian principles. *Scientific Reports*, 13(1), 2023.
- [8] Agrim Gupta, Silvio Savarese, Surya Ganguli, and Li Fei-Fei. Embodied intelligence via learning and evolution. *Nature Communications*, 12(1), 2021.
- [9] Leni K. Le Goff, Edgar Buchanan, Emma Hart, Agoston E. Eiben, Wei Li, Matteo De Carlo, Alan F. Winfield, Matthew F. Hale, Robert Woolley, Mike Angus, Jon Timmis, and Andy M. Tyrrell. Morpho evolution with learning using a controller archive as an inheritance mechanism. *IEEE Transactions on Cognitive and Developmental Systems*, 15(2):507–517, June 2023.
- [10] Amir Behjat, Krushang Khimjibhai Gabani, Chen Zeng, and Souma Chowdhury. Concurrent morphology-optimization and behavior-learning: Co-designing intelligent quadcopters. In *AIAA AVIATION 2020 FORUM*. AIAA, 2020.
- [11] Chen Zeng, Prajit KrisshnaKumar, Jhoel Witter, and Souma Chowdhury. Efficient concurrent design of the morphology of unmanned aerial systems and their collective-search behavior. In *IEEE/RSJ International Conference on Intelligent Robots and Systems, IROS 2022, Kyoto, Japan, October 23-27*, 2022, pages 388–393. IEEE, 2022.
- [12] Fabio Bergonti, Gabriele Nava, Valentin Wüest, Antonello Paolino, Giuseppe L'Erario, Daniele Pucci, and Dario Floreano. Co-design optimisation of morphing topology and control of winged drones, 2024.
- [13] Danial Sufiyan, Luke Soe Thura Win, Shane Kyi Hla Win, Gim Song Soh, and Shaohui Foong. Joint mechanical design and flight control optimization of a nature-inspired unmanned aerial vehicle via collaborative co-evolution. *IEEE Robotics and Automation Letters*, 6(2):2044–2051, 2021.
- [14] A. E. Eiben and J.E. Smith. Introduction to Evolutionary Computing. Springer-Verlag, London, 2003. 2nd edition in 2015.
- [15] Elijah H. W. Ang, Christophe De Wagter, and Guido C. H. E. de Croon. Multi-objective evolution of drone morphology, 2025.
- [16] Franz Rothlauf and David E Goldberg. Prüfer numbers and genetic algorithms: A lesson on how the low locality of an encoding can harm the performance of GAs. In *International Conference on Parallel Problem Solving from Nature*, pages 395–404. Springer, 2000.
- [17] Jens Gottlieb and Günther R Raidl. Characterizing locality in decoder-based EAs for the multidimensional knapsack problem. In *European Conference on Artificial Evolution*, pages 38–52. Springer, 1999.
- [18] Franz Rothlauf and David Goldberg. Tree network design with genetic algorithms—an investigation in the locality of the pruefernumber encoding. In *Late Breaking Papers at the Genetic and Evolutionary Computation Conference*, pages 238–244, 1999.
- [19] John Schulman, Filip Wolski, Prafulla Dhariwal, Alec Radford, and Oleg Klimov. Proximal policy optimization algorithms. *ArXiv*, abs/1707.06347, 2017.
- [20] Antonin Raffin, Ashley Hill, Adam Gleave, Anssi Kanervisto, Maximilian Ernestus, and Noah Dormann. Stable-baselines3: Reliable reinforcement learning implementations. *Journal of Machine Learning Research*, 22(268):1–8, 2021
- [21] Robin Ferede, Till Blaha, Erin Lucassen, Christophe De Wagter, and Guido C. H. E. de Croon. One net to rule them all: Domain randomization in quadcopter racing across different platforms, 2025.
- [22] H. W. Kuhn. The Hungarian method for the assignment problem. *Naval Research Logistics Quarterly*, 2(1-2):83–97, 1955.
- [23] Fuda van Diggelen, Eliseo Ferrante, and A. E. Eiben. Comparing Robot Controller Optimization Methods on Evolvable Morphologies. *Evolutionary Computation*, pages 1–20, 08 2023.